A Study of Rotational Movement and Charging Torque of Reconfigured On-Board Charger

Yang Xiao, *Student Member, IEEE*, and Chunhua Liu, *Senior Member, IEEE*

***Abstract*—This article studies the rotational movement and charging torque in a new reconfigured on-board charger during the charging process. Recently, the reconfigured on-board charger becomes attractive because the propulsive units are engaged in the charging system to reduce the cost and volume. Since the unbalanced currents flow through the three-phase permanent-magnet synchronous machine, the rotational movement and charging torque are generated. The charging torque may be equal to the rated propulsive torque at some special rotor positions, which is unsafe and may lead to the rotational movement, extra noise, and motor wear. In order to reduce the influence of charging torque and rotational movement during the charging process, the charging torque is analyzed based on the magnetic coenergy. It is found that the charging torque is related to the unbalanced current, differential-mode current, and current ripple in motor windings. Thus, the mutual inductances of motor windings during the charging process are decoupled into the differential-mode and common-mode inductances. Furthermore, a solution is provided to significantly minimize the charging torque based on the control methods of the ac/dc side and dc/dc side. Finally, the experimental results are provided to verify the correctness of the suppression of rotational movement and the charging performance.**

***Index Terms*—Charging torque, electric drive, electric vehicle (EV), on-board charger, permanent-magnet machine, rotational movement, three-phase motor.**

I. Introduction

THE propulsive system and charging system for electric vehicle (EV) are usually designed separately. In particular, the power converters, control units, and cooling parts for the propulsive and charging systems are designed in different packages, which results in the high cost and large volume [1], [2]. One solution to overcome this problem is to integrate the propulsive components into the charging units, which is termed as the reconfigured on-board charger [3].

Manuscript received May 28, 2019; revised September 8, 2019, November 16, 2019, and January 11, 2020; accepted March 3, 2020. Date of publication March 8, 2020; date of current version June 23, 2020. This work was supported in part by a grant of Shenzhen–Hong Kong Innovation Circle Category D Project from the Science Technology and Innovation Committee of Shenzhen Municipality, China, under Project SGDX2019081623101559, in part by the grants from the Innovation and Technology Commission, Hong Kong, under Projects ITS/353/16 and ITP/027/19AP, and in part by the Teaching Development Grant and CityU Strategic Research Grant from the City University of Hong Kong, Hong Kong, under Project TDG6000675, Project SRG11218317, and Project SRG11218519. Recommended for publication by Associate Editor Q. Li. *(Corresponding author: Chunhua Liu.)*

The authors are with the School of Energy and Environment, City University of Hong Kong, Kowloon, Hong Kong (e-mail: ansel.shaw@my.cityu.edu.hk; chunliu@cityu.edu.hk).

Color versions of one or more of the figures in this article are available online at http://ieeexplore.ieee.org.

Digital Object Identifier 10.1109/TPEL.2020.2979349

Some pioneers have explored the reconfigured on-board charger with publications and patents [4]–[6]. Among them, two main directions are usually considered as the reconfigured on-board EV chargers. The first direction is that the traction inverter and motor windings are reused as the rectifier and grid-side filter in an on-board charger. In [7], a three-phase induction machine was reused as a transformer, while a rectifier was used to charge the vehicle battery. A similar situation was found in [8], where the motor windings were reused as the grid-side filters. However, a brake was adopted in both [7] and [10] to prevent the motor rotation because independent charging and propulsive systems can lead to large three-phase alternating currents flowed through the windings of the induction machine. In [9]–[12], multiphase machines and multiphase inverters were integrated into the charging system. Additional phase-shifted transformer [8], complex current-rearrangement devices [10], [11], or center-tapped motor windings [12] were needed to prevent the charging torque generation, which increased the system complexity and volume. In [13], an effective charging torque elimination method is proposed for a six-phase integrated on-board charger. Six-phase motor windings and traction inverter are reused as the rectifier filters and six-phase rectifier. It suppressed the charging torque when ac currents flow through the six-phase motor windings. In [11], an alternative configuration that did not require any hardware reconfiguration for the battery charger was presented. It reused a nine-phase traction machine and a nine-phase traction inverter as a nine-phase rectifier and grid-side filters. However, there would be uncertainty to install multiphase machines in EVs since semiconductor devices and sensors need to be doubled or even tripled compared with a three-phase traction system.

Another direction is to reuse the traction inverter and the motor windings as a dc/dc converter and dc-side filter with an additional front-end rectifier. In [14] and [15], a switched reluctance machine (SRM) drive system was integrated into the dc/dc side, but the SRM was not mainstream for the present EV application due to the torque ripple and operation noise. In [16], it emphasized the small battery current ripple in the on-board charger and it was based on the interleaved control strategy. However, the motor vibration and noise might be produced if the current ripples in the motor windings were too large. In this way, the long-term machine wear would reduce the machine reliability and service time. In [17], the traction inverter was reused as a three-phase dc/dc converter, where an additional high-frequency inductor was installed between the end of the motor winding and battery to reduce the common-mode current. However, an additional device added difficulty and complexity to integrate into an existing battery charger. Furthermore, a differential-mode current is not considered as a factor of the

rotational movement. In [18], a single-phase on-board charger was derived from a three-phase drive system in which the inverter served as a single-phase dc/dc converter and two phases of the motor windings were used as a series-wound inductor. However, the current of one motor winding was zero, while the currents of the other windings were the same. Hence, the charging torque and rotational movement by a fixed angle may occur due to the unbalanced motor winding currents and unfortunately no comment was made in the article.

In addition, there are also multifunctional integrated systems for the battery charger. In [19] and [20], a three-phase split-winding SRM-drive system was reconfigured as a multifunctional converter. Two phases of the drive system were reused as a single-phase rectifier, while the left phase served as a single-phase dc/dc converter. In [21], a nine-phase traction system was integrated into the battery charger, where six phases of the motor windings are reused as the grid-side filters and the remaining three-phase windings were used as dc/dc inductors. Meanwhile, the nine-phase traction inverter was reutilized as a six-phase rectifier and a three-phase chopper. The common problem of multifunctional integrated systems is that the machine type is special and seldom used in EVs. Furthermore, the charging torque elimination method in multifunctional integrated charger is complex, which raises difficulty in manufacturing. In [27], a current-source-integrated battery charger is proposed and the motor windings are also used as inductors. However, more diodes and grid-side capacitors are adopted compared with the voltage-source-integrated battery charger.

This article studies a three-phase permanent-magnet synchronous machine (PMSM) reconfigured on-board charger, which reutilizes the inverter for propulsion as a dc/dc converter to avoid the complex integration in [9]–[12]. In order to eliminate an extra inductor in [17], two-phase motor windings of the three-phase machine are reutilized as the dc/dc inductors, while the remaining phase serves as a common-mode inductor to maintain good charging performance. However, in this way, the rotational movement is detected in the proposed on-board charger. Thus, the universal charging torque is analyzed to solve this problem. The unbalanced currents, differential-mode current, and current ripple in motor windings are first proved to affect the charging torque and rotational movement. Thereby, the mutual inductances of motor windings during the charging process are decoupled into the differential-mode and common-mode inductances. Moreover, the control methods of the rectifier side, the differential-mode controller, and the position control are developed to reduce the charging torque. Finally, a testbed of three-phase PMSM-integrated on-board charger is built. The experimental results are provided to prove the validity of the suppression of rotational movement in a reconfigured on-board charger.

II. Theoretical Analysis

Fig. 1(a) shows the existing system configuration of an EV that contains a propulsive unit and an on-board charging unit. The existing EV has separate power converters, control units, and cooling units for the propulsive and charging systems, which is not economical but easy to implement. In contrast, Fig. 1(b) demonstrates the proposed propulsion/charging system for EV in which only a relay K_3 is added to shift between the charging

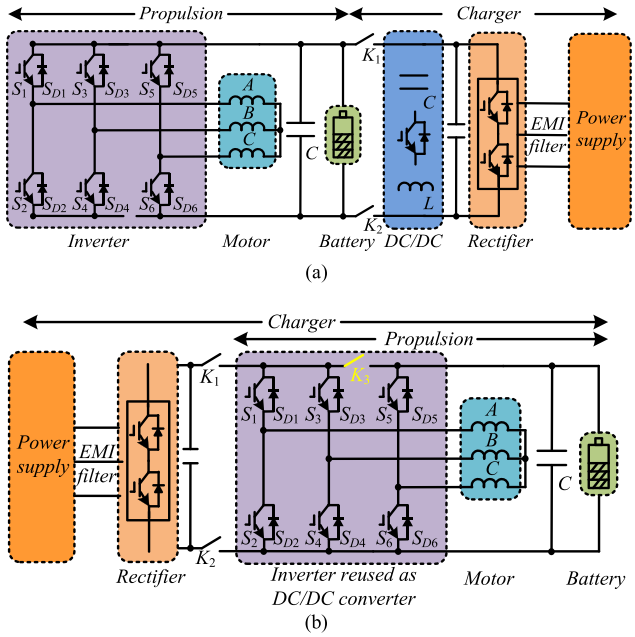

Fig. 1. Electrical system configuration of EV. (a) Existing EV propulsion/charging system. (b) Proposed EV propulsion/charging system.

mode and the propulsive mode. During the propulsive process, the connectors K_1 and K_2 are OFF, while the K_3 is ON. During the charging process, the K_1 and K_2 are ON, while K_3 is OFF. It needs to mention that a relay or bidirectional power switch can be used as K_3. The relay is installed on printed circuit boards (PCBs), which reduces the connection length and stray inductance compared with the other cable connections.

When compared with the on-board chargers, the proposed EV system reserves the existing propulsive unit and exploits it to the maximum function for charging. First, the semiconductor devices of the dc/dc part in Fig. 1(a) are saved by reutilizing the inverter as a dc/dc converter. This initiative economizes considerable cost in the car manufacture as the semiconductor devices for EV application are quite expensive. Second, two motor windings of a three-phase machine serve as the dc/dc inductors, while the remaining phase serves as a common-mode inductor. This saves space as the inductors with high current capacity are bulky [17]. Third, the microchip, cooling system, current, and voltage hall sensors for propulsion are also integrated into the proposed charging system. Hence, the cost and volume of the proposed EV system are vastly reduced.

A. Operation Principle

Fig. 2 demonstrates four current patterns of the inverter, which are termed as Mode I, Mode II, Mode III, and Mode IV. Although the dc currents flow through the motor windings, the motor phase currents may be coupled with each other due to large current ripples and mutual inductances. The flux of the three-phase PMSM machine is modeled as [22]

$$\psi = \begin{bmatrix} L_A & L_{AB} & L_{AC} \\ L_{BA} & L_B & L_{BC} \\ L_{CA} & L_{CB} & L_C \end{bmatrix} \begin{bmatrix} i_A \\ i_B \\ i_C \end{bmatrix} + \psi_{fd} \begin{bmatrix} \cos(\theta_e) \\ \cos(\theta_e - 2\pi/3) \\ \cos(\theta_e - 4\pi/3) \end{bmatrix} \tag{1}$$

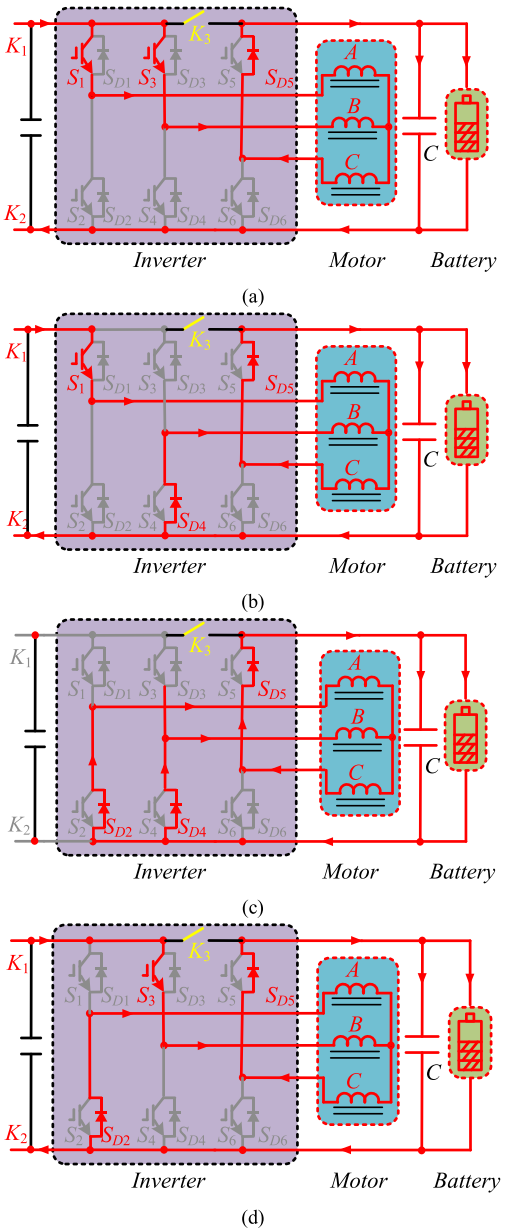

Fig. 2. Current flow patterns of inverter. (a) Mode I. (b) Mode II. (c) Mode III. (d) Mode IV.

where i_A, i_B, and i_C are the currents of three-phase motor windings, ψ_{fd} and θ_e are the permanent-magnet flux and electric angle, respectively. L_A, L_B, and L_C are the main inductances, while L_{AB}, L_{BA}, L_{AC}, L_{CA}, L_{BC}, and L_{CB} are the mutual inductances. The relationships between mutual inductances are

$$L_{AB} = L_{BA}, \quad L_{AC} = L_{CA}, \quad L_{BC} = L_{CB}. \tag{2}$$

The phase voltages of the motor windings are obtained by

$$\begin{bmatrix} u_A \\ u_B \\ u_C \end{bmatrix} = \begin{bmatrix} R_A & & \\ & R_B & \\ & & R_C \end{bmatrix} \begin{bmatrix} i_A \\ i_B \\ i_C \end{bmatrix} + \begin{bmatrix} L_A & L_{AB} & L_{AC} \\ L_{BA} & L_B & L_{BC} \\ L_{CA} & L_{CB} & L_C \end{bmatrix} \begin{bmatrix} \frac{di_A}{dt} \\ \frac{di_B}{dt} \\ \frac{di_C}{dt} \end{bmatrix} \tag{3}$$

where R_A, R_B, and R_C are the resistances of motor windings, u_A, u_B, and u_C are the phase voltages of motor windings.

The motor phase currents are divided into differential-mode currents and common-mode currents, where i'_A and i'_B are the differential-mode currents, and i_{AC}, i_{BC}, and i_{CC} are the common-mode currents

$$\begin{bmatrix} i_A \\ i_B \\ i_C \end{bmatrix} = \begin{bmatrix} i'_A \\ i'_B \\ 0 \end{bmatrix} + \begin{bmatrix} i_{AC} \\ i_{BC} \\ i_{CC} \end{bmatrix}. \tag{4}$$

The differential-mode current does not exist in phase-*C* and the differential currents in phase-*A* and phase-*B* are

$$i'_A + i'_B = 0. \tag{5}$$

The common-mode currents in phase-*A* and phase-*B* are

$$i_{AC} = i_{BC} = -\frac{i_{CC}}{2}. \tag{6}$$

Thus, the motor phase voltages are rewritten by substituting (4) into (3)

$$\begin{bmatrix} u'_A \\ u'_B \end{bmatrix} = \begin{bmatrix} R_A & \\ & R_B \end{bmatrix} \begin{bmatrix} i'_A \\ i'_B \end{bmatrix} + \begin{bmatrix} L_A - L_{AB} & \\ & L_B - L_{BA} \end{bmatrix} \times \begin{bmatrix} \frac{di'_A}{dt} \\ \frac{di'_B}{dt} \end{bmatrix} \tag{7}$$

$$\begin{bmatrix} u_{AC} \\ u_{BC} \\ u_{CC} \end{bmatrix} = \begin{bmatrix} R_A & & \\ & R_B & \\ & & R_C \end{bmatrix} \begin{bmatrix} i_{AC} \\ i_{BC} \\ i_{CC} \end{bmatrix} + \begin{bmatrix} L_A + L_{AB} - 2L_{AC} & 0 & 0 \\ 0 & L_B + L_{BA} - 2L_{BC} & 0 \\ 0 & 0 & L_C - \frac{L_{AC}+L_{CB}}{2} \end{bmatrix} \begin{bmatrix} \frac{di_{AC}}{dt} \\ \frac{di_{BC}}{dt} \\ \frac{di_{CC}}{dt} \end{bmatrix} \tag{8}$$

where u'_A and u'_B are the differential-mode voltages, while u_{AC}, u_{BC}, and u_{CC} are the common-mode voltages. Fig. 3 shows the equivalent circuits of the three-phase PMSM in charging mode.

It is worth mentioning that the demagnetization of the permanent magnets due to the large dc winding currents during the EV battery charging process is not going to happen. The EV charging power for family use is usually below 20 kW, which is much smaller than the propulsive power (Nissan 2018 LEAF: 110 kW). Hence, the motor winding currents for propulsion are much larger than the currents for charging. In addition, the cooling system is also shared in the proposed on-board charger and the heat dissipation capability is enough for the proposed application. Thus, the demagnetization of the propulsive motor due to high currents and high temperatures will not occur.

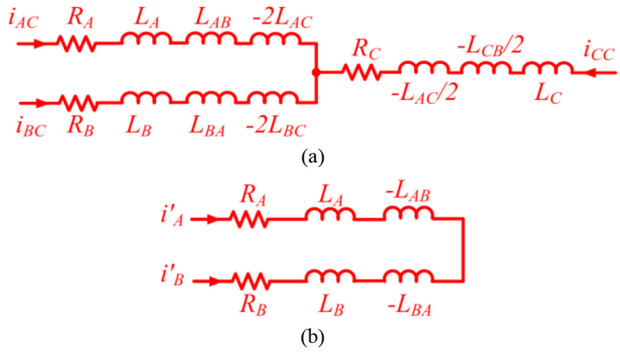

Fig. 3. Models of a three-phase machine in the charging process. (a) Common mode. (b) Differential mode.

B. Charging Torque Analysis

The rotational movement is related to the charging torque, which is different from the propulsive torque as the motor does not rotate in the proposed reconfigured system. In addition, the propulsive torque is calculated based on the transformation of *abc–dq* axis, while the transformation for the reconfigured charging system is not needed. Thus, the universal charging torque is calculated based on the magnetic coenergy (W'_m) [23]. If the winding currents $i_1, \ldots, i_n$ and the electric angle θ_e serve as the independent variables, the magnetic coenergy [23]–[25] is defined as

$$W'_m(i_1, i_2, \ldots, i_n, \theta_e) = \sum_1^n i_k \psi_k - W_m(\psi_1, \psi_2, \ldots, \psi_n, \theta_e) \tag{9}$$

where W_m is the magnetic energy and $\psi_1, \ldots, \psi_n$ are the flux linkages of *n* windings. The magnetic coenergy is

$$\begin{aligned} W'_m = &\int_0^{i_1} \psi_1(i'_1, 0, \ldots, 0, \theta_e) di'_1 \\ &+ \int_0^{i_2} \psi_2(i_1, i'_2, 0, \ldots, 0, \theta_e) di'_2 \\ &+ \cdots + \int_0^{i_n} \psi_n(i_1, i_2, \ldots, i'_n, \theta_e) di'_n. \end{aligned} \tag{10}$$

The torque [21]–[23] is defined as

$$T_e = n_p \frac{\partial W'_m}{\partial \theta_e} \tag{11}$$

where θ_{mech} is the mechanical angle, which follows $\theta_{\text{mech}} = \theta / n_p$. n_p is the number of pole pairs.

If the motor is a PMSM, the magnetic coenergy is

$$\begin{aligned} W'_m = &\frac{1}{2} L_{11}(\theta_e) i_1^2 + \frac{1}{2} L_{22}(\theta_e) i_2^2 + \cdots + \frac{1}{2} L_{nn}(\theta_e) i_n^2 \\ &+ L_{12}(\theta_e) i_1 i_2 + L_{13}(\theta_e) i_1 i_3 + \cdots + L_{n,n-1}(\theta_e) i_n i_{n-1} \\ &+ i_1 \psi_{fd} \cos(\theta_e) + i_2 \psi_{fd} \cos\left(\theta_e - \frac{2\pi}{n}\right) \\ &+ \cdots + i_n \psi_{fd} \cos\left(\theta_e - \frac{2(n-1)\pi}{n}\right). \end{aligned} \tag{12}$$

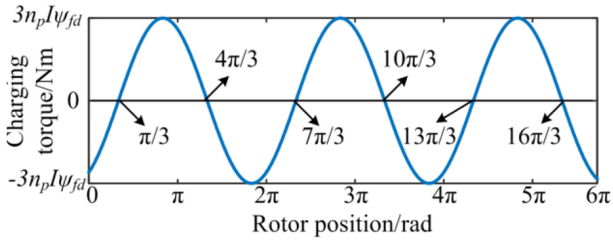

Fig. 4. Charging torque at different rotor positions.

Thus, the universal charging torque in matrix form is

$$T_e = n_p \left(i_s^T \psi_{fd} \frac{\partial \gamma}{\partial \theta_e} + \frac{1}{2} i_s^T \frac{\partial L_s}{\partial \theta_e} i_s \right) \tag{13}$$

where L_s is the motor inductance matrix and $\gamma = [\cos(\theta_e) \cos(\theta_e - 2\pi/n) \cdots \cos(\theta_e - 2(n-1)\pi/n)^T$.

The inductance matrix of a three-phase motor is available in [26] and [27], which consists of the leakage inductance L_1, zero-sequence inductance L_0, and second-order magnetizing inductance L_2.

$$\begin{aligned} L_s &= \begin{bmatrix} L_A & L_{AB} & L_{AC} \\ L_{BA} & L_B & L_{BC} \\ L_{CA} & L_{CB} & L_C \end{bmatrix} \\ &= L_1 \begin{bmatrix} 1 & 0 & 0 \\ 0 & 1 & 0 \\ 0 & 0 & 1 \end{bmatrix} + L_0 \begin{bmatrix} 1 & -0.5 & -0.5 \\ -0.5 & 1 & -0.5 \\ -0.5 & -0.5 & 1 \end{bmatrix} \\ &\quad + L_2 \begin{bmatrix} \cos 2\theta_e & \cos 2(\theta_e - \frac{\pi}{3}) & \cos 2\left(\theta_e + \frac{\pi}{3}\right) \\ \cos 2(\theta_e - \frac{\pi}{3}) & \cos 2(\theta_e + \frac{\pi}{3}) & \cos 2\theta_e \\ \cos 2(\theta_e + \frac{\pi}{3}) & \cos 2\theta_e & \cos 2\left(\theta_e - \frac{\pi}{3}\right) \end{bmatrix}. \end{aligned} \tag{14}$$

According to (13), if the charging currents of each-phase windings are the same, such as $i_A = i_B = i_C = I$, the charging torque equals zero. It means that the machine does not produce torque during the charging process. However, the currents of the motor windings in the proposed EV system are not the same. So, a rotational charging torque generates at the beginning of the charging process until the forces are balanced. It is assumed that the dc components of charging currents are $i_A = i_B = I$, $i_C = -2I$. Thus, the charging torque related to the rotational movement should be

$$T_e = 3 n_p I \psi_{fd} \sin(\theta_e - \pi/3). \tag{15}$$

Fig. 4 demonstrates the relationship between the charging torque and the rotor position. The charging torque fluctuates around zero and it is related to the rotor position. In some positions, the charging torque is $3n_pI\psi_{fd}$, which is nearly equal to the rated torque of propulsion. Hence, the charging torque is unsafe and needs to be suppressed. It is also observed that the charging torque is zero at some rotor positions, for example, $\pi/3$ and $4\pi/3$. This position is termed as a safe charging position.

Furthermore, the differential-mode current may also affect the charging torque. If the differential-mode current in phase-*A* and phase-*B* is ΔI, the component of charging torque related to the

differential-mode current is

$$T_{e\_\text{differential}} = \sqrt{3} n_p \Delta I \psi_{fd} \sin(\theta_e + \pi/6). \quad (16)$$

In addition, high-frequency current components affect the generation of the charging torque; the major components of the high-frequency components are assumed as follows:

$$\begin{cases} i_{A\_\text{high}} = I_{h1} \sin(\omega t + \phi) + I_{h3} \sin(3\omega t + \phi) \\ i_{B\_\text{high}} = I_{h2} \sin(\omega t + \phi) + I_{h4} \sin(3\omega t + \phi) \\ i_{C\_\text{high}} = -i_{LA\_\text{high}} - i_{LB\_\text{high}} \end{cases} \quad (17)$$

where I_{h1}, I_{h2}, I_{h3}, and I_{h4} are the amplitudes of the current ripples, and ω and φ are the frequency and phase position of the current ripple, respectively. The ripple charging torque at the safe charging position is

$$T_{e\_\text{ripple}} = \frac{\sqrt{3}}{2} n_p \psi_{fd} [(I_{h1} - I_{h2}) \sin(\omega t + \phi) + (I_{h3} - I_{h4}) \sin(3\omega t + \phi)]. \quad (18)$$

Generally, an EV is designed as the "park and charge" solution, which means the vehicle stops and parks first and then the consumer needs to take off the vehicle and plug in the connector. If the rotor is not at the calculated safe charging position, such as $\pi/3$ position, the motor is possible to produce enough charging torque to rotate the rotor by a certain distance. It is unacceptable and unsafe that the vehicle moves.

In summary, the charging torque is not zero at the beginning of the charging process if the rotor position is not at the safe charging position. The motor will produce a rotational movement until the electromagnetic force and the friction force are balanced. This rotational movement could be nearly equal to the rated propulsive torque, as a result of which the vehicle may be out of control during the charging process. Also, the differential-mode current between phase-*A* and phase-*B* needs to be controlled as an offset of the safe charging position will be produced. In addition, ripple torque caused by ripple charging currents needs to be paid attention as large ripple torque may lead to vibration and noise.

III. Control Algorithm

Fig. 5 shows the global control diagram of the proposed reconfigured on-board charger. The rotor position control is conducted before charging. The control algorithm during charging includes the ac/dc-side control and the dc/dc-side control. The ac/dc-side control contains the power factor control and the dc-link voltage control, which is combined by space vector modulation. The dc/dc-side control contains the differential-mode current control and the state-of-charge control.

A. AC/DC-Side Control

A phase-locked loop (PLL) is used to track the phase position of the grid voltage to achieve a unit power factor operation. In PLL, the static coordinate transformation is used to transfer the variables from the *abc*-axis to $\alpha\beta$-axis. Then, the variables in the $\alpha\beta$-axis are transferred into the *dq*-axis, which is termed as the rotating coordinating transformation.

Fig. 6 demonstrates the control diagram of the ac/dc side. The control method can realize the unit power factor operation by adopting the three proportional–integral control loops. First, the

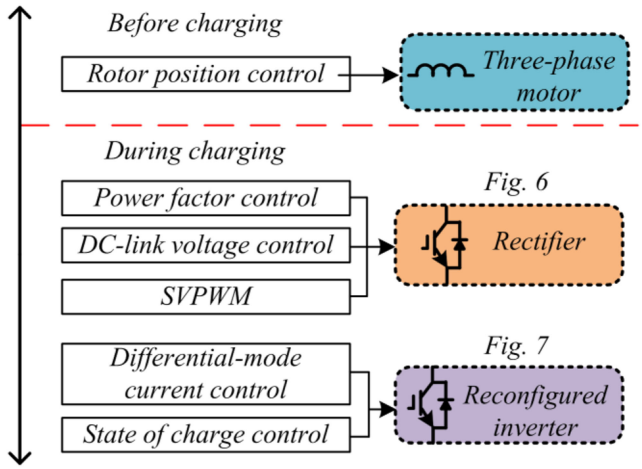

Fig. 5. Global control diagram.

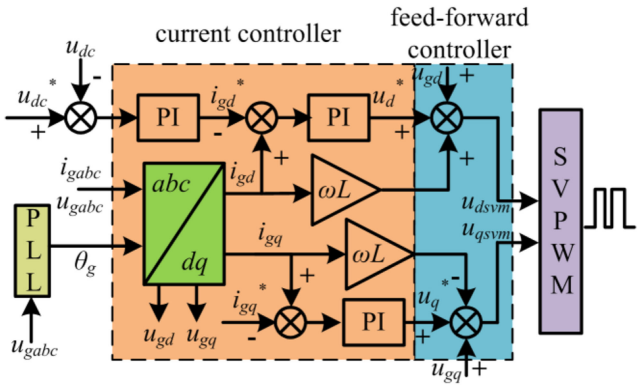

Fig. 6. Control diagram for ac/dc side.

error between the desired voltage value and the actual value is used to obtain the reference value of the *d*-axis grid current i_{gd}^*. In order to meet the unit power factor operation, the reference *q*-axis current of the grid side i_{gq}^* is set at zero. In addition, the space vector pulsewidth modulation (SVPWM) is used to improve the grid current performance. Finally, the *dq* components of the SVPWM voltage ($u_{d\text{svm}}$, $u_{q\text{svm}}$) are modulated to generate the pulsewidth (PWM) modulation signals.

The dynamic characteristic of the *dq* components in control loops will interact with each other due to the coupling factor in inductors after the coordinate transformation [28]. In order to eliminate the interaction, the feed-forward decoupling controller is used in the charging system to decouple the *dq*-axis components completely.

B. DC/DC-Side Control

Traditionally, the charging voltage and current ripples are the foremost things in a battery charger. Also, the interleaved method is adopted as it optimizes the output ripple current [29], [30]. However, it is not the same case in the proposed reconfigured on-board charger as the differential-mode currents need to be eliminated.

It needs to mention that phase-*C* of the motor winding is used as a common-mode inductor in the proposed charging system. Thus, compared with the dc/dc converter, the phase-*C* motor winding is able to provide further optimized charging

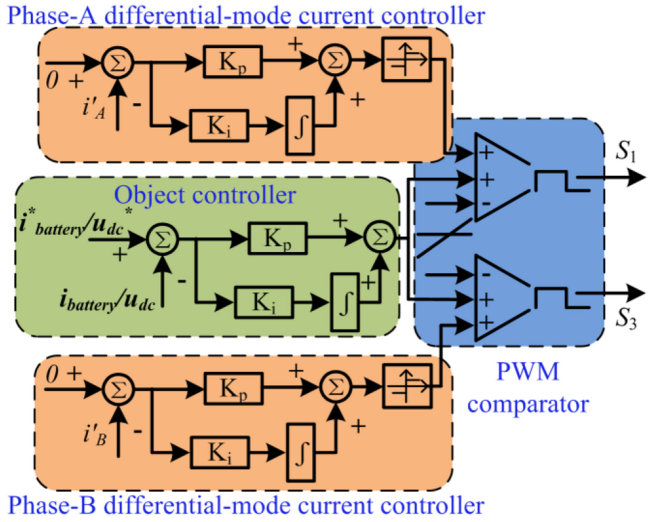

Fig. 7. Control method of dc/dc side.

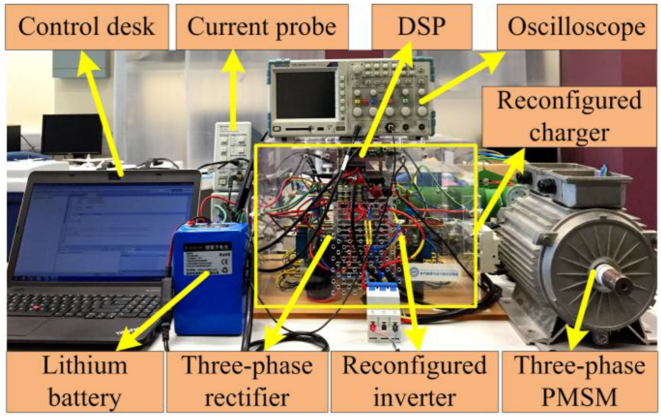

Fig. 8. Experimental prototype of the proposed reconfigured on-board charger.

TABLE I
KEY PARAMETERS OF THE PROPOSED ON-BOARD CHARGER

Parameters	Values
Carrier frequency	20kHz
Motor type	PMSM
Rated motor power	4kW
Max motor current	Over 10A
Rated motor speed	3000rpm
No. pole pairs	3
Rated motor frequency	150Hz
Inductance of motor winding L_A (20kHz)	1.059mH
Resistance of motor winding R_A	0.482Ω
Mutual inductance of motor winding L_{AB} (20kHz)	0.031mH
Inductance of motor winding L_B (20kHz)	1.001mH
Resistance of motor winding R_B	0.515Ω
Mutual inductance of motor winding L_{BC} (20kHz)	0.062mH
Inductance of motor winding L_C (20kHz)	1.067mH
Resistance of motor winding R_C	0.487Ω
Mutual inductance of motor winding L_{AC} (20kHz)	0.044mH
Li-Battery	48V 10Ah

performance for the battery charger. Furthermore, the performance of charging and propulsion would be better if the mutual inductance of the motor windings is optimized to a smaller one. In this way, the decoupled design of currents is not needed. Moreover, the high common-mode inductance of the motor winding is good for charging performance to obtain small ripple current.

Fig. 7 shows the control method in the dc/dc side, which contains an object controller, two differential-mode current controllers, and two PWM comparators. First, the object controller is designed to reach the reference charging states, such as constant current (CC) charging or constant voltage (CV) charging. Second, the differential-mode current controllers are designed to eliminate the differential-mode current resulted from the differential-mode inductances as the differential-mode current will produce an offset of the safe charging position and increase copper loss in the motor. Hence, the reference values of differential-mode currents are set at zero, while the upper and lower saturation limits are used to prevent overmodulation. Finally, the output PWM signals are generated by comparing the duty cycles and carrier waves in the PWM comparators.

To park the vehicle at the safe charging position, a rotor position orientation method is conducted, whose precision is up to the resolution ratio of the encoder. In fact, the position control is mature in servo control. A closed position loop is enough to be added outside the field-oriented control loop in motor drives, which is textbook materials [31]. Other advanced methods can also be found in the pieces of literature, such as [13] and [32].

IV. RESULT ANALYSIS

A scale-down three-phase on-board charger is built to verify the above-mentioned analysis and charging performance. Fig. 8 illustrates the main units in the proposed on-board charger, which includes the three-phase PMSM reconfigured on-board charger, battery, control desk, oscilloscope, and probes. The three-phase on-board charger consists of the buck-type converter, three-phase boost-type rectifier, three-phase PMSM, hall sensors, a digital signal processor, and drive circuits.

The designed voltage of ac input is 380 V, the dc-link voltage is 600–700 V, and the battery voltage is about 400 V. However, a 48 V 10 Ah lithium battery is used as the charging object due to the lack of a real EV battery pack. Hence, an isolated transformer is adopted to lower down the input voltage as it is unnecessary to charge a 48 V battery with 380 V ac-grid voltage. However, the isolated transformer is no longer needed at the designed rating. A 12-V, 200-A relay K_3 is installed on the PCB board and the size is $46 * 46 * 44.5$ mm.

It also needs to mention that the power switches of a traction inverter need to be rated differently (high voltage for charging mode, but high current in propulsion mode), and the dc-link capacitor also needs to be higher voltage rated as well as the rectifier devices compared with the traditional approach. Thus, global considerations are needed when selecting suitable power switches and capacitors for one EV with integrated function.

The motor inductance changes at different operating frequencies due to the magnetic conductivity. Hence, the motor inductances of windings are retested under 20 kHz, which is the operating frequency of the dc/dc converter. The key parameters are listed in Table I.

Fig. 9(a) shows the grid-side performance of the reconfigured on-board charger. The transformer-side voltage is 36.5 V and

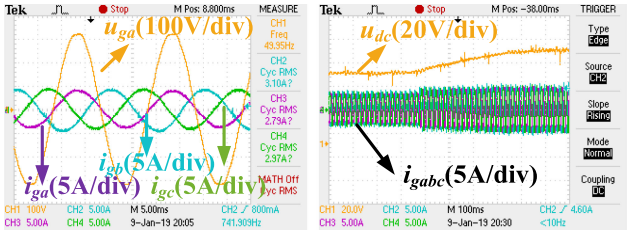

(a) (b)

Fig. 9. Grid-side performance of the on-board charger. (a) Grid voltage and three-phase currents. (b) Sudden variation.

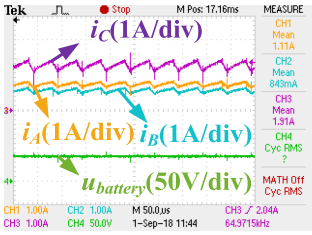

Fig. 10. CC charging performances of the proposed control without differential-mode current controllers.

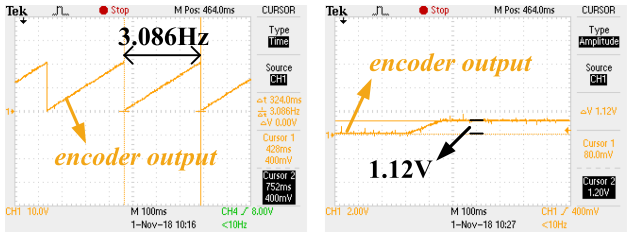

(a) (b)

Fig. 11. (a) Encoder output with 185 r/min. (b) Encoder output of position control.

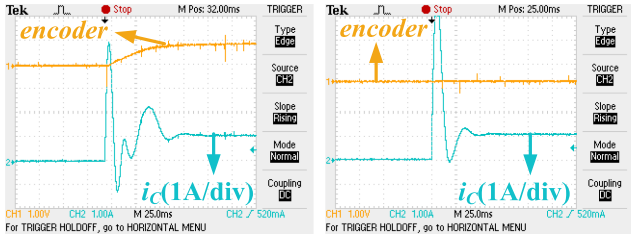

(a) (b)

Fig. 12. Encoder output at the beginning of the charging process. (a) At a random position. (b) At the safe charging position.

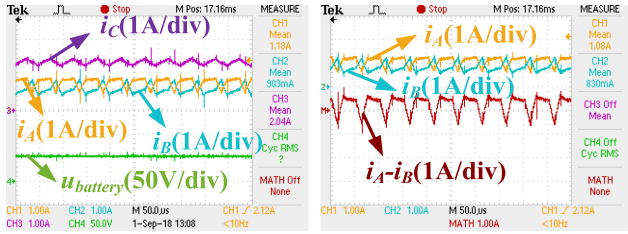

(a) (b)

Fig. 13. CC charging performances of an interleaved method.

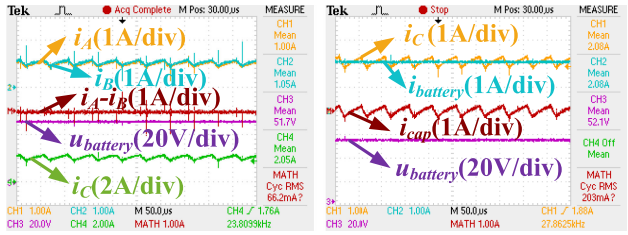

(a) (b)

Fig. 14. CC charging performances at the safe charging position.

the reference dc-link voltage is 70 V. It is observed that the input currents are in-phase with the grid voltage, which exhibits the effect of the power factor correction. Fig. 9(b) shows the grid-side performance during the sudden variation, where the reference dc-link voltage increases from 60 to 75 V.

Fig. 10 demonstrates the CC charging performance without a differential-mode current controller. The currents in phase-*A* and phase-*B* motor winding are not balanced, which results from the differential-mode currents. The unbalanced currents in phase-*A* and phase-*B* windings would generate an offset of the position control; as a result, the rotational movement and extra copper loss will be generated.

Fig. 11(a) shows the encoder output of the propulsive mode at about 185 r/min. The digital to analog (DA) output changes from 0 to 20 V for a motorcycle. Fig. 11(b) shows the encoder output of the position control. The rotor starts from 0° and stops at 60.48° (1.12/20 ∗ 360 ∗ 3), which is very close to the calculated 60°. In the proposed reconfigured charger, a 2048DPI encoder is used in the position control and it is quite common and cheap in the automotive application. The actual accuracy is about ±0.05 mechanical angle, which is enough for precise position control. In addition, the resolution depends on the motor poles. For the motor with more poles, a more precise encoder is needed as the safe charging positions increase in a 360 mechanical angle. There is also a little tolerance for position control due to friction and cogging torque.

Fig. 12 simulates the rotational movement when 1 A constant charging current flows through the motor windings. Fig. 12(a) shows the encoder output at the beginning of the charging process when the rotor is not at the safe charging position. It is observed that the rotational movement occurs, which may lead to unsafe factors. Fig. 12(b) shows that the rotor remains standstill when the rotor is at the safe charging position.

Fig. 13 shows the charging performance of the interleaved method under 2 A CC charging. Fig. 13(a) shows the motor winding currents and battery voltage. The current ripples of the three-phase motor windings are 0.28, 0.28, and 0.15 A. Fig. 13(b) shows the difference of the currents in phase-*A* and phase-*B* windings, which is twice the differential-mode current, as analyzed in (5). The difference-mode current ripple is 0.13 A. Similarly, the unbalanced phase-*A* and phase-*B* currents may lead to unsafe factors during the charging process. Hence, the interleaved method is not suitable for the proposed charger.

Fig. 14(a) exhibits the charging performance of the three-phase windings, differential-mode current, and battery voltage under 2-A CC charging at the safe charging position. The current ripples of the motor windings are 0.1, 0.1, and 0.2 A. The current

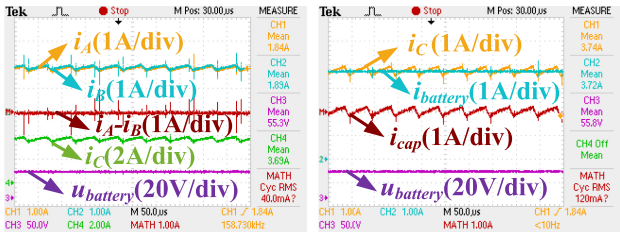

Fig. 15. CV charging performances at the safe charging position.

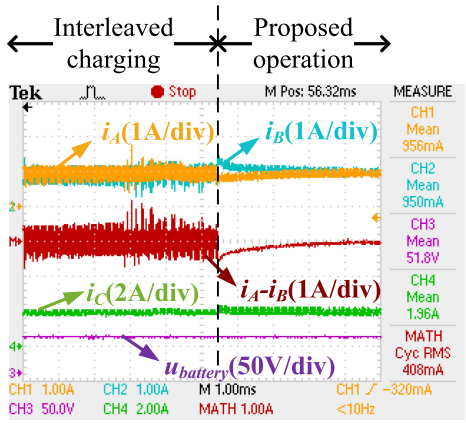

Fig. 16. Comparison of the interleaved charging method and the proposed method.

ripples in phase-*A* and phase-*B* are reduced compared with the interleaved method because of the common-mode inductor in phase-*C*. In addition, the differential-mode current ripple is almost zero, which shows that the charging torque is almost zero. The balanced currents in phase-*A* and phase-*B* guarantee the safe operation of the proposed reconfigured on-board charger. Fig. 14(b) shows the battery charging current, capacitor current, and battery voltage, which are stable and robust. The differences in the battery voltage in different figures are normal as it increases slowly with the battery capacity.

Fig. 15 shows the charging performance under CV charging at the safe charging position. The battery voltage is set at 55 V and it remains constant with around 0.3 V ripple. The current ripples of motor windings are 0.09, 0.09, and 0.18 A. The differential-mode current ripple is about zero, which means phase-*A* and phase-*B* winding currents are uniform. Similarly, the uniform charging currents in phase-*A* and phase-*B* are necessary to keep the rotor stable at the safe charging position as discussed.

Fig. 16 demonstrates the comparison between the two methods when the interleaved method transfers to the proposed method. It is observed clearly that the current ripples in phase-*A* and phase-*B* windings reduce sharply, while the current ripple in phase-*C* winding increases slightly. Furthermore, the differential-mode current ripple decreases to zero, which shows the effect of the differential-mode current controller. The stable motor winding currents without differential-mode currents can guarantee the rotor to locate at the safe charging positions.

Fig. 17(a) shows the overall efficiency of the proposed integrated on-board charger at 2 kW due to the current limitation of motor windings. Fig. 17(b) shows the estimated loss of each part. It is observed that the motor winding loss is the major

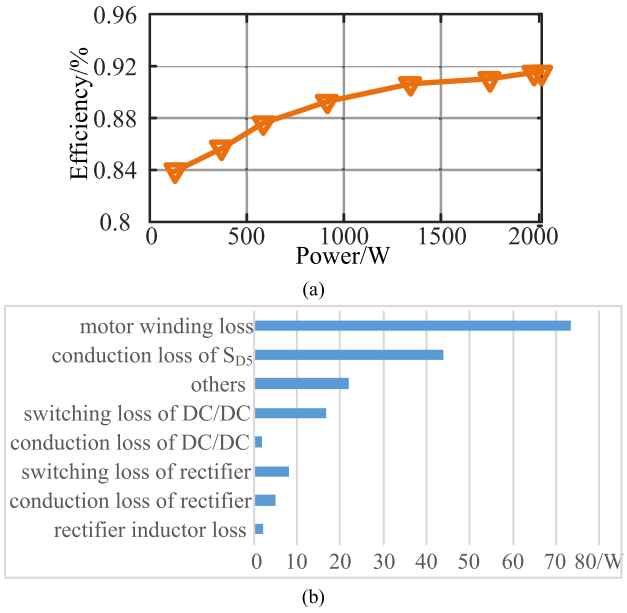

Fig. 17. (a) Efficiency of the proposed integrated on-board charger. (b) Loss estimation at 2 kW.

loss due to the reutilization of motor windings. In addition, the conduction loss of S_{D5} is also large due to the structure of the reconfigured on-board charger. The forward voltage of S_{D5} is about 4.4 V and the current is about 10 A. A more advanced power switch with smaller forward voltage will be better for efficiency improvement. The "others" are mainly about the power loss of the drive circuits.

V. Conclusion

In this article, a new three-phase PMSM reconfigured on-board charger and its charging torque and rotational movement are studied. The main contributions are summarized as follows.

1) A new reconfigured on-board charger is proposed to avoid the complex integration. By adding a single relay in the inverter, two phases of the motor windings are reutilized as the dc/dc inductors, while the remaining phase serves as a common-mode inductor. Meanwhile, two phases of the inverter serve as a dc/dc converter, while the other phase is reused as a conduction path.
2) In order to eliminate the initial movement and noise during the charging process, the mechanism of charging torque is analyzed. Furthermore, the mutual inductance of motor windings in the charging process is decoupled into the common-mode and differential-mode inductance as the unbalanced current is proved to affect the initial movement.
3) The control method of ac/dc is developed to achieve the unity power factor correction. Moreover, the charging performances at the safe charging positions are elaborated in detail.
4) A testbed of the proposed reconfigured on-board charger is built up. The experimental results show the validity and feasibility of the proposed on-board charger and charging torque analysis.

REFERENCES

[1] S. Haghbin, S. Lundmark, M. Alakula, and O. Carlson, "Grid-connected integrated battery chargers in vehicle applications: Review and new solution," *IEEE Trans. Ind. Electron.*, vol. 60, no. 2, pp. 459–473, Feb. 2013.

[2] J. de Santiago *et al.*, "Electrical motor drivelines in commercial all-electric vehicles: A review," *IEEE Trans. Veh. Technol.*, vol. 61, no. 2, pp. 475–484, Feb. 2012.

[3] S. S. Williamson, A. K. Rathore, and F. Musavi, "Industrial electronics for electric transportation: Current state-of-the-art and future challenges," *IEEE Trans. Ind. Electron.*, vol. 62, no. 5, pp. 3021–3032, May 2015.

[4] M. Yilmaz and P. T. Krein, "Review of battery charger topologies, charging power levels, and infrastructure for plug-in electric and hybrid vehicles," *IEEE Trans. Power Electron.*, vol. 28, no. 5, pp. 2151–2169, May 2013.

[5] A. G. Cocconi, "Combined motor drive and battery recharge system," U.S. Patent 5 341 075, Aug. 23, 1994.

[6] J. Hoon, J. Byung, W. Jang, J. Ki, J. Chun, and S. Yang, "Inverter-charger integrated device for electric vehicle," U.S. Patent 961 676 0B2, Apr. 11, 2017.

[7] F. Lacressonniere and B. Cassoret, "Converter used as a battery charger and a motor speed controller in an industrial truck," in *Proc. Eur. Conf. Power Electron. Appl.*, Dresden, Germany, 2005, pp. 1–7.

[8] D. Zhuolin, Z. Feng, C. Wei, W. Yongxing, Z. Dong, and W. Xuhui, "Analysis of charging torque in a three-phase integrated charger of electrical vehicle," in *Proc. IEEE Conf. Expo. Transp. Electrific. Asia-Pac.*, Beijing, China, 2014, pp. 1–5.

[9] I. Subotic, N. Bodo, E. Levi, M. Jones, and V. Levi, "Isolated chargers for EVs incorporating six-phase machines," *IEEE Trans. Ind. Electron.*, vol. 63, no. 1, pp. 653–664, Jan. 2016.

[10] I. Subotic, N. Bodo, and E. Levi, "An EV drive-train with integrated fast charging capability," *IEEE Trans. Power Electron.*, vol. 31, no. 2, pp. 1461–1471, Feb. 2016.

[11] N. Bodo, E. Levi, I. Subotic, J. Espina, L. Empringham, and C. M. Johnson, "Efficiency evaluation of fully integrated on-board EV battery chargers with nine-phase machines," *IEEE Trans. Energy Convers.*, vol. 32, no. 1, pp. 257–266, Mar. 2017.

[12] W. Lhomme *et al.*, "Integrated traction/charge/air compression supply using three-phase split-windings motor for electric vehicles," *IEEE Trans. Power Electron.*, vol. 33, no. 11, pp. 10003–10012, Nov. 2018.

[13] Y. Xiao, C. Liu, and F. Yu, "An effective charging-torque elimination method for six-phase integrated on-board EV chargers," *IEEE Trans. Power Electron.*, vol. 35, no. 3, pp. 2776–2786, Mar. 2020.

[14] H.-C. Chang and C.-M. Liaw, "Development of a compact switched-reluctance motor drive for EV propulsion with voltage-boosting and PFC charging capabilities," *IEEE Trans. Veh. Technol.*, vol. 58, no. 7, pp. 3198–3215, Sep. 2009.

[15] Y. Hu, X. Song, W. Cao, and B. Ji, "New SR drive with integrated charging capacity for plug-in hybrid electric vehicles (PHEVs)," *IEEE Trans. Ind. Electron.*, vol. 61, no. 10, pp. 5722–5731, Oct. 2014.

[16] Y.-S. Lin, K.-W. Hu, T.-H. Yeh, and C.-M. Liaw, "An electric-vehicle IPMSM drive with interleaved front-end DC/DC converter," *IEEE Trans. Veh. Technol.*, vol. 65, no. 6, pp. 4493–4504, Jun. 2016.

[17] Y. Xiao, C. Liu, and F. Yu, "An integrated on-board EV charger with safe charging operation for three-phase IPM motor," *IEEE Trans. Ind. Electron.*, vol. 66, no. 10, pp. 7551–7560, Oct. 2019.

[18] T.-H. Liu, Y. Chen, P.-H. Yi, and J.-L. Chen, "Integrated battery charger with power factor correction for electric-propulsion systems," *IET Electr. Power Appl.*, vol. 9, no. 3, pp. 229–238, Mar. 2015.

[19] J. Liang, W. Li, Z. Song, and Y. Shi, "An integrated battery charger base on split-winding switched reluctance motor drive," in *Proc. IEEE Transp. Electrific. Conf. Expo., Asia-Pac.*, Busan, South Korea, 2016, pp. 106–111.

[20] J. G. Hayes, "Battery charging systems for electric vehicles," in *Proc. IEE Colloq. Electr. Veh. - Technol. Roadmap Future*, London, U.K., 1998, pp. 4/1–4/8.

[21] F. Yu, W. Zhang, Y. Shen, and J. Mao, "A nine-phase permanent magnet electric-drive-reconstructed onboard charger for electric vehicle," *IEEE Trans. Energy Convers.*, vol. 33, no. 4, pp. 2091–2101, Dec. 2018.

[22] W. Wang, J. Zhang, M. Cheng, and S. Li, "Fault-tolerant control of dual three-phase permanent-magnet synchronous machine drives under open-phase faults," *IEEE Trans. Power Electron.*, vol. 32, no. 3, pp. 2052–2063, Mar. 2017.

[23] J. F. Gieras, C. Wang, and J. C. Lai, *Noise of Polyphase Electric Motors*. Boca Raton, FL, USA: CRC Press, 2018.

[24] K. Fukushima, S. A. Nasar, and R. M. Saunders, "Electromechanical energy conversion in salient-pole structures," *IEEE Trans. Power App. Syst.*, vol. 82, no. 68, pp. 760–766, Oct. 1963.

[25] T. A. Lipo, *Analysis of Synchronous Machines*. Boca Raton, FL, USA: CRC Press, 2017.

[26] G. Pellegrino, E. Armando, and P. Guglielmi, "An integral battery charger with power factor correction for electric scooter," *IEEE Trans. Power Electron.*, vol. 25, no. 3, pp. 751–759, Mar. 2010.

[27] C. Shi, Y. Tang, and A. Khaligh, "A three-phase integrated onboard charger for plug-in electric vehicles," *IEEE Trans. Power Electron.*, vol. 33, no. 6, pp. 4716–4725, Jun. 2018.

[28] M. S. Diab, A. A. Elserougi, A. S. Abdel-Khalik, A. M. Massoud, and S. Ahmed, "A nine-switch-converter-based integrated motor drive and battery charger system for EVs using symmetrical six-phase machines," *IEEE Trans. Ind. Electron.*, vol. 63, no. 9, pp. 5326–5335, Sep. 2016.

[29] D. B. W. Abeywardana, P. Acuna, B. Hredzak, R. P. Aguilera, and V. G. Agelidis, "Single-phase boost inverter-based electric vehicle charger with integrated vehicle to grid reactive power compensation," *IEEE Trans. Power Electron.*, vol. 33, no. 4, pp. 3462–3471, Apr. 2018.

[30] H.-C. Chen, C.-Y. Lu, and L.-M. Huang, "Decoupled current-balancing control with single-sensor sampling-current strategy for two-phase interleaved boost-type converters," *IEEE Trans. Ind. Electron.*, vol. 63, no. 3, pp. 1507–1518, Mar. 2016.

[31] K. Gulez, A. A. Adam, and H. Pastaci, "Torque ripple and EMI noise minimization in PMSM using active filter topology and field-oriented control," *IEEE Trans. Ind. Electron.*, vol. 55, no. 1, pp. 251–257, Jan. 2008.

[32] R. Shahnazi, H. M. Shanechi, and N. Pariz, "Position control of induction and DC servomotors: A novel adaptive fuzzy PI sliding mode control," *IEEE Trans. Energy Convers.*, vol. 23, no. 1, pp. 138–147, Mar. 2008.

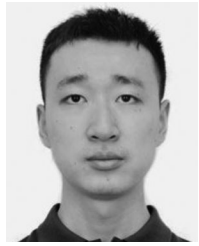

Yang Xiao (Student Member, IEEE) received the B.Eng. degree in electrical engineering and automation from Soochow University, Suzhou, China, in 2014, and the M.Eng. degree in electrical engineering from Southeast University, Nanjing, China, in 2017. He is currently working toward the Ph.D. degree with the City University of Hong Kong, Kowloon, Hong Kong.

His main research interests include power electronics, wireless power transmission, electric vehicle battery charger, and control of multiphase drive systems.

Chunhua Liu (Senior Member, IEEE) received the B.Eng. and M.Eng. degrees in automatic control from the Beijing Institute of Technology, China, in 2002 and 2005, respectively, and the Ph.D. degree in electrical and electronic engineering, The University of Hong Kong, Hong Kong SAR, in 2009.

He is currently an Assistant Professor of electrical and electronic engineering with the School of Energy and Environment, City University of Hong Kong, Kowloon, Hong Kong. His research interests include electric machines and drives, electric vehicles and aircrafts, electric robotics and ships, renewables and microgrid, power electronics, and wireless power transfer. In these areas, he has authored or coauthored more than 200 refereed papers.

Dr. Liu is currently an Associate Editor for the IEEE TRANSACTIONS ON INDUSTRIAL ELECTRONICS, and an Editor for the IEEE TRANSACTIONS ON VEHICULAR TECHNOLOGY and the IEEE TRANSACTIONS ON ENERGY CONVERSION. He is also a Subject Editor for the *IET – Renewable Power Generation*, a Subject Editor of Cambridge University – *Wireless Power Transfer*, an Editor for *Energies* and the IEEE TRANSACTIONS ON MAGNETICS—Conference, and an Associate Editor for the IEEE Open Journal of the Industrial Electronics Society and the *IEEE Chinese Journal of Electrical Engineering*. In addition, he is a Chair and a Founder of Hong Kong Chapter, IEEE Vehicular Technology Society.